RSC Advances

ROYAL SOCIETY OF CHEMISTRY

www.rsc.org/advances

Journal Name

ARTICLE

Superior Optical Response of Size-controlled Silicon Nano-crystals in a-Si:H/nc-Si:H Superlattice Films for Multi-junction Solar Cells

Received 00th January 20xx,
Accepted 00th January 20xx

DOI: 10.1039/x0xx00000x

www.rsc.org/

Debjit Kar and Debajyoti Das*

In order to facilitate widening in optical band-gap utilizing quantum size-effects in silicon nanocrystals (Si-ncs) of few nanometers in dimension, self-assembled Si-ncs embedded in a-Si matrix were grown within a-Si:H/nc-Si:H superlattice (SL) thin films produced by alternating sub-layers of a-Si:H and nc-Si:H from (SiH_4+H_2)-plasma in PE-CVD at 180°C, without post-deposition annealing. Growth of Si-ncs extending all through the nc-Si:H sub-layer thickness are terminated by alternate deposition of a-Si:H barrier-layer during each cycle and the average size of Si-ncs with narrow size-distribution are tuned by controlling each nc-Si:H sub-layer thickness. Significantly high-density tiny Si-ncs are grown even within ultra-thin (~3 nm) nc-Si:H sub-layer and that has been made possible via an ingenious approach, by utilizing the underneath a-Si:H sub-layer as the virtual incubation-layer at the very specifically chosen parametric condition, during each cycle of periodic deposition. On systematic thinning of nc-S:H active-layer within 8–3 nm, remarkable increase in optical absorption at near-UV photon energies along with simultaneous optical band-gap widening within 1.89–2.04 eV demonstrate the quantum size-effect on Si-ncs to play the key role. Subsequent lowering in the defect-states identifies the nc-Si:H/a-Si:H SL-films as a superior material for using in devices, including as *i*-layers in triple-junction all-silicon solar cells.

Introduction

Self-assembled silicon nano-crystals (Si-ncs) embedded in a superlattice structure or in dielectric matrix is a fascinating area of research in the field of materials science due to the potential applications of such structures in photovoltaics, optoelectronics, light emitting devices and photo-detectors.[1-6] Taking the advantage of the quantum confinement effect due to the size reduction of Si-ncs towards few nanometers, the band gap of the materials can be well-tuned. In third generation silicon solar cells with triple tandem structure, the top cell should have the highest band gap (~2.0 eV) and the two subsequent cells need to have sequentially lower band gaps in order to enable efficient absorption of the solar spectrum.[7, 8] The different band gap for each *i*-layer can be achieved by modifying the confinement potential of Si-ncs by tuning their average size. In implementing such scheme, superior control over the size of Si-ncs and their distribution are the prerequisite. In that direction, there are many approaches available in the literature, e.g. forming nano-crystals in dielectric matrix (a-SiO_x, a-SiC or a-SiN) by plasma enhanced CVD (both capacitively and inductively coupled),[9-12] hotwire CVD or by layer-by-layer deposition mostly using RF magnetron sputtering.[7] Among those, nano-scaled superlattice structures with alternate Si-rich layer and Si_3N_4/SiO_2/SiC dielectric layer have attracted substantial attention as they provide superior control over the growth of Si-ncs [2] which, however, proceeds essentially through high temperature post-deposition annealing at ~1100 °C.[13-16] On annealing, solid-phase crystallization in the Si-rich layer leads to the formation of Si-ncs and their size-evolution is constrained by the thickness of the Si-rich sub-layer within the dielectric barriers on both sides. This inevitable high temperature annealing step imposes a persistent hindrance in its successful application in thin film solar cells and restriction on the use of low cost substrates, and also affects the other pre-deposited layers of the device. In addition, the charge carriers are obstructed by the high dielectric barriers on both sides of the Si-rich layer. In order to minimize the obstruction, the dielectric layers should be thin and the Si-ncs should be closely spaced so as to allow the overlapping of the wave-functions in between the adjacent Si-ncs.[2] In this regard, low temperature deposition of superlattice films with sub-layers of hydrogenated amorphous silicon (a-Si:H) and nano-crystalline silicon (nc-Si:H) that contains Si-ncs of size controlled by the corresponding sub-layer thickness, without post deposition annealing, could be significantly important in terms of improving the carrier transport due to lower dielectric barrier of a-Si:H sub-layer, and making device fabrication feasible at low deposition temperature. In addition, the a-Si:H/nc-Si:H superlattice thin films with quantum-well structure, when used as the active layer in hot carrier solar cells, could be instrumental in cooling down of the hot carriers exploiting the band gap difference between its sub-layers.[17]

Nano-Science Group,
Energy Research Unit,
Indian Association for the Cultivation of Science,
Jadavpur, Kolkata – 700 032, INDIA
E-mail (D. Das): erdd@iacs.res.in; Fax: +91(33)24732805

Accordingly, in this investigation, we demonstrate a straightforward synthesis to fabricate superlattice thin films consisting of alternate sub-layers of a-Si:H and nc-Si:H at low temperature of ~180 ^{o}C, from (SiH_4 + H_2)-plasma in capacitively coupled plasma enhanced CVD. Significant widening in the optical band gap of the superlattice films has been tried to attain utilizing the quantum size effects on tiny Si-ncs the size of which are tuned by controlling the thickness of the nc-Si:H active layer within the a-Si:H barrier layers, without any post-deposition annealing.

Experimental Details

The superlattice (SL) thin films consisting of repeated cycles of alternate sub-layers of hydrogenated amorphous silicon (a-Si:H) and hydrogenated nanocrystalline silicon (nc-Si:H) were fabricated from hydrogen diluted silane (SiH_4 + H_2) plasma using a 13.56 MHz capacitively coupled plasma enhanced chemical vapor deposition (CC PE-CVD) system. The deposition conditions for each individual sub-layer (a-Si:H and nc-Si:H) were separately optimized in thick layers, prior to preparation of the superlattice samples. For the deposition of the alternate layers all the deposition parameters were changed except the substrate temperature which was maintained at 180^{o}C. The pressure, power, H_2 and SiH_4 flow were kept as 3 Torr, 15 W, 95 sccm and 5 sccm, respectively for a-Si:H layer and 4 Torr, 40 W, 99.5 sccm and 0.5 sccm for nc-Si:H layer. For different SL-thin films, the thickness of the nc-Si:H layers (t_{nc}) was changed from 3 nm to 8 nm, by varying the deposition time, while the thickness of the a-Si:H layers remained unchanged at 4.8 nm. The SL-thin films were deposited on Corning® Eagle2000^{TM} glass substrates for various structural and optical studies. Each SL-thin film consisted of a-Si:H sub-layers on both ends and the total thickness of each sample, including the bulk layers, was maintained constant at ~ 200 nm, by changing the number of bi-layers. A schematic diagram for sample preparation steps along with representative superlattice structure has been depicted in Figure 1(a) and 1(b).

The thickness of the samples was estimated using a Dektak 6M profilometer. Small angle X-ray diffractometry with incident beam at glancing angle (GISAX) was performed with Cu K_α X-ray radiation (λ=1.5418 Å) source in Bruker (D8 Advance) system. The Raman spectrum was obtained at room temperature in a backscattering geometry using a triple Raman spectrometer (J-Y Horiba, Model No. T64000) with an excitation wavelength of 514 nm from a water-cooled Ar^+ laser source (Spectra Physics made), at a low power density of 2 mWcm^{-2}. The beam spot was focused inside the SL-thin films by Olympus open stage microscope and the scattered signal was detected by TE-cooled CCD camera. The optical density data of the samples were obtained from absorption and reflection measurements in the UV-visible region at room temperature, using a double beam spectrophotometer (Hitachi330, Japan). Transmission electron microscopy was performed using a JEOL JSM 2010 transmission electron microscope operating at 200 kV.

Results

Small-Angle XRD

The structural periodicity of the a-Si:H/nc-Si:H superlattice (SL) thin films has been estimated from the small-angle XRD data obtained within limited 2Θ-span of 0.5° to 4.0°, at glancing angle of incidence (GISAX), for varying thickness of the nc-Si:H active layer (t_{nc}) while maintaining a constant thickness of the a-Si:H dielectric barrier layer (t_a). Figure 2 shows the 1st order (m=1) diffraction peak at 2Θ= 1.10° of the SL-thin film for t_{nc}=3 nm, which arises due to the periodic appearance of the combination of active-layer and barrier layer of (t_{nc} + t_a) thickness for a number of repeated cycles, forming a superlattice structure of the thin film. On increase in the periodic thickness of the superlattice by elevating t_{nc} from 3 to 4 nm, the 1st order diffraction peak is no more detectable due to the angular-limitation of SAX measurement instruments. The 2nd order (m=2) peaks for t_{nc}=4 nm, 6 nm and 8 nm are observed at 2Θ = 1.96°, 1.76° and 1.46°, respectively. It is notable that the diffraction peak positions shifted systematically towards lower diffraction angle (2Θ) because of regular thickening of periodic layers. Ultimately, the small angle X-ray diffraction results demonstrate the systematic formation of proper superlattice structures in the present set of thin films.

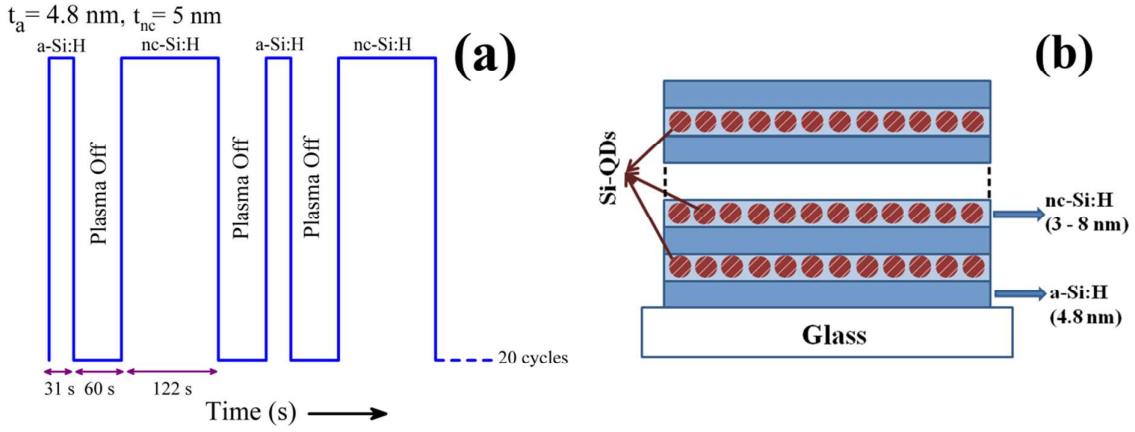

Figure 1. (a) A representative deposition scheme of the a-Si:H/nc-Si:H superlattice thin films. (b) Schematic diagram of the superlattice structure with alternate layers of a-Si:H and nc-Si:H.

Journal Name

ARTICLE

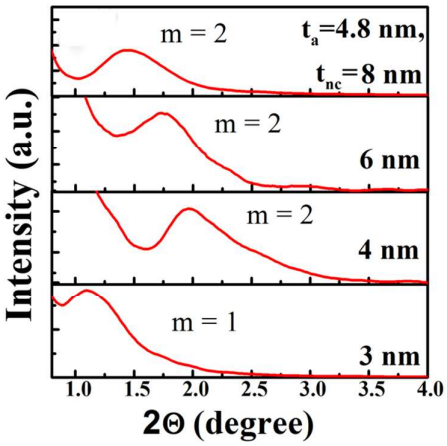

Figure 2. Small angle X-ray diffraction spectra of a-Si:H/nc-Si:H superlattice thin films with different thickness (t_{nc}) of nc-Si:H active sub-layer showing 1st and 2nd order diffraction peaks.

Raman Spectroscopy

Raman spectroscopy is one of the most useful and non-destructive optical tool for the characterization of nano-crystalline properties of silicon. Figure 3(a) presents the normalized Raman spectra for the set of films with different t_{nc}. In general, each Raman spectrum appears to possess four individual components, viz, three broad components around ~310 cm^{-1}, ~420 cm^{-1} and 480 cm^{-1}, known as LA, LO and TO Raman modes of amorphous silicon (a-Si)[18] and the fourth sharp peak at ~518 cm^{-1} as the TO Raman mode of crystalline silicon (c-Si). It has been grossly noted that with the systematic increase in the nanocrystalline active layer thickness, t_{nc}, the intensity of the TO Raman mode of a-Si component gradually reduced and the reduction appeared quite significant for t_{nc} > 6 nm, while the peak of the TO Raman mode of nc-Si component gradually sharpened and shifted towards higher wave numbers. As per the available literature on nc-Si, an intermediate component at around 500-510 cm^{-1} has been considered which was assigned to the thermodynamically stable very tiny nano-crystallites of Si (ultra-nanocrystalline silicon, unc-Si) and/or the grain-boundary region,[19-21] a prominent signature of which is evident in the spectrun for t_{nc} ≤6 nm. A representative deconvolution of all the five satellite components has been shown in the inset of Figure 3(a).

The crystalline volume fraction (F_c) has been estimated using the following formula:

$$F_c = \frac{I_{nc} + I_{unc/gb}}{I_{nc} + I_{unc/gb} + \beta I_a}$$

where, I_{nc}, I_{unc} and I_a are the integrated area of the peaks corresponding to nc-Si, unc-Si and a-Si components, respectively. Considering the average size of the nanocrystallites in the order of few nano-meters, β, the ratio of cross-sections between crystalline and amorphous components, has been taken unity.[22] Figure 2(b), demonstrates that a reasonably high crystalline volume fraction (F_c) ~42% has been obtained in the SL film even with very low periodic thickness of the nc-Si:H active layer, t_{nc} ~3 nm. With systematic increase in t_{nc}, F_c increases gradually and attains a very high magnitude ~67.4% for t_{nc}= 8 nm. Thus the a-Si:H/nc-Si:H SL film with a periodic thickness (t_a + t_{nc}) = (4.8 + 8) nm, produces an almost continuously grown nc-Si:H network in terms of sufficiently high degree of the overall crystallinity.

Considering the nc-Si satellite component of the Raman peak, in particular, obtained from the deconvolution of the Raman spectra, Figure 3(c) demonstrates that the nc-Si peak gradually becomes broader in FWHM along with continuous shift towards lower wave numbers, from 518.7 to 513 cm^{-1} on systematic thinning in t_{nc} from 8 to 3 nm. This shift of the nc-Si peak position can be attributed to the phonon confinement effect in silicon nano-crystallites.[23] For bulk crystalline silicon (c-Si), the first order Raman scattering process of the excited phonon has been limited at the centre

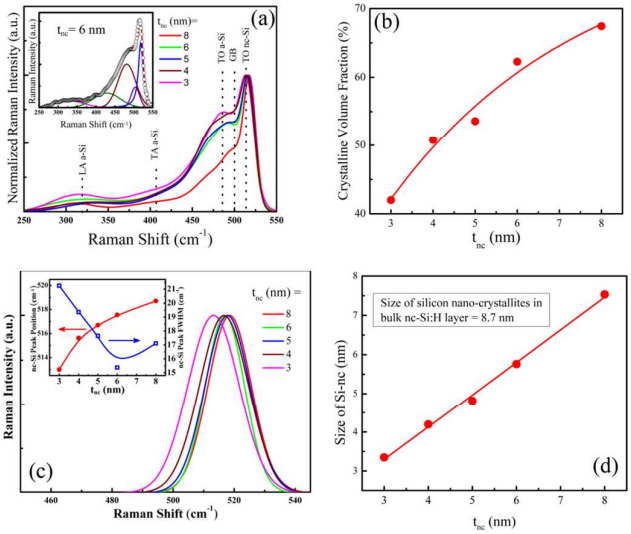

Figure 3. (a) Normalized Raman spectra for superlattice thin films with different t_{nc}. Inset shows the typical deconvolution of the Raman spectra into satellite components. (b) The enhanced crystalline volume fraction on widening of t_{nc}. (c) The deconvoluted spectra of the nc-Si component, showing gradual blue-shift at lower t_{nc}. Inset shows the variation of the peak position and FWHM of nc-Si peak. (d) The average size of silicon nano-crystals, as calculated from the position of nc-Si peak, being larger at increasing t_{nc}.

of Brillouin zone by the momentum conservation law. However, with the formation of Si-ncs, the phonons, dispersed over the Brillouin zone, started contributing in Raman spectra due to spatial confinement of phonons within the Si-ncs by the presence of structural defects at nano-crystalline boundaries. This phonon confinement effect caused the shift of the nc-Si peak position towards lower wave numbers, along with the broadening of its line-width. Strong confinement effects occurred when the radius of the Si-ncs approached the Bohr's radius of silicon (~5 nm) and reduced further. Considering the shift of nc-Si peak arising due to the size-variation of Si-ncs and assuming the spherical shape of the Si-ncs, their average size can be estimated by the empirical formula:[18]

$$d = 2\pi\left(\frac{2}{\Delta\omega}\right)^{1/2}$$

where, $\Delta\omega$ is the relative shifting of the nc-Si peak position from 520 cm^{-1} (corresponding to bulk c-Si). Figure 3(d) demonstrates that the average size (d) of Si-ncs gradually increased from ~3.3 to ~7.5 nm as t_{nc} was enhanced from 3 to 8 nm. It is notable that the average grain sizes (d), as estimated from Raman spectroscopy, are comparable with the thickness (t_{nc}) of the nc-Si:H active layer sandwiched between two adjacent a-Si:H barrier layers. According to the phonon confinement effect, the size-reduction of Si-ncs induces shifting of the peak position towards lower wave numbers along with widening in the line-width of the peak. Contrary to that effect, as seen in Figure 3(c), the FWHM of the nc-Si peak widened from 15.54 to 17.11 cm^{-1} as t_{nc} was increased from 6 to 8 nm. Actually, in contrary to the effect of phonon confinement mentioned above, narrower size distribution opposes the peak broadening. The FWHM of the nc-Si peak is thus governed by two competitive factors – the reduction in the average size of Si-ncs widens the FWHM while the narrow size-distribution of Si-nc opposes this widening. In the range, 6 nm $\leq t_{nc} \leq$ 8 nm, the average grain size varied in the range 5.7 nm $\leq d \leq$ 7.5 nm where quantum confinement do have its feeble effects in the limit of Bohr's radius, while size distribution effects may play significantly.[24] It has been identified by the TEM studies mentioned in the next section that the size distribution became narrower when the grain size reduced within thinner t_{nc}, which might be supported by similar earlier reports as well.[10] Thus the deviation of the FWHM data-point for t_{nc}= 8 nm from the regular nature of its variation in Figure 3(c) is reasonably explained, while for t_{nc}<6 nm, strong phonon confinement effect became dominant over the effect of narrow size-distribution, that finally resulted in prominent broadening of nc-Si peak.[25]

TEM analysis

Systematic variations in the evolution of silicon nano-crystals (Si-ncs) in the a-Si:H/nc-Si:H SL-films on increase in the periodic thickness (t_{nc}) of the nc-layers, have been studied by transmission electron microscopy (TEM). The TEM samples have been prepared on carbon coated Cu-grids with a common initial amorphous layer of thickness t_a=4.8 nm and the 3 and 2 bi-layers each of (t_{nc} + t_a) thickness for films with t_{nc}=5 nm and 8 nm, respectively, in order to maintain a gross thickness >30 nm in each case. The plain view TEM micrograph for the SL-thin films with t_{nc}= 5 nm, in Figure 4(a-i) identifies the deep dark spots as the Si-ncs which are uniformly distributed in the relatively bright a-Si matrix. On increase in nc-layer thickness t_{nc} to 8 nm, the micrograph in Figure 4(b-i) shows the growth of relatively large size of the Si-ncs which are closely packed and bound by sharp edges with narrow amorphous interconnections. Individual lattice planes of c-Si are clearly identified in the HR-TEM micrographs in Figure 4(a-ii) and (b-ii). The corresponding selected area electron diffraction pattern (SAED), shown in the inset of Figure 4(a-i) exhibit diffraction rings corresponding to <111> and <220> planes of c-Si, while similar SAED pattern for t_{nc}=8 nm, in the inset of Figure 4(b-i) exhibits relative sharp diffraction rings implying the formation of relatively enhanced crystallinity with <111>, <220> and <311> planes of Si.

The histogram plots in Figure 4(a-iii) and (b-iii) for t_{nc}=5 and 8 nm respectively, present the nearly Gaussian distribution of the Si-ncs with corresponding FWHMs as 4.34 and 6.03 nm, respectively, demonstrating narrower size distribution of the Si-ncs in thinner nc-Si:H layers. On increase in nc-Si:H layer thickness (t_{nc}) from 5 to 8 nm, the average size (d) of Si-ncs, obtained from the apex of the Gaussian distribution, increases from ~5.5 to ~8.1 nm, along with corresponding increase in number density from ~3.5 × 10^{10} cm^{-2} to ~7.5 × 10^{10} cm^{-2}, respectively. It is, therefore, significant to

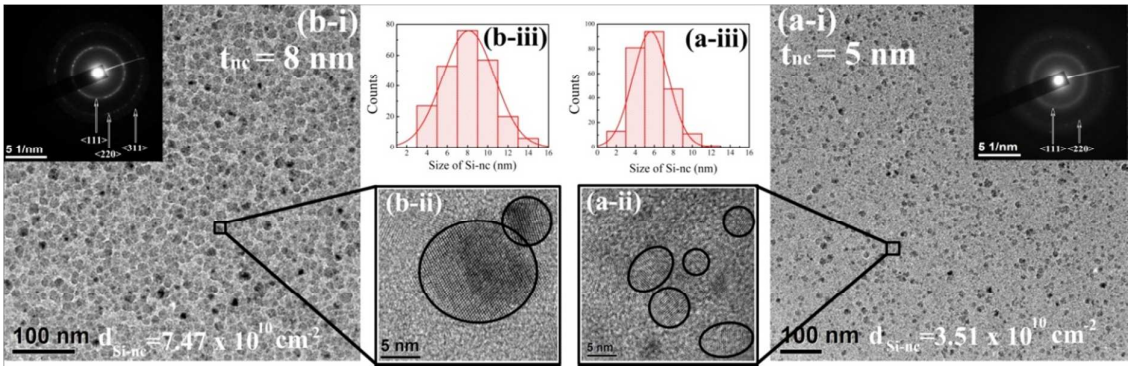

Figure 4. (a-i) and (b-i) The plain view TEM micrographs of the a-Si:H/nc-Si:H superlattice thin films with t_{nc}=5 and 8 nm. Insets present the related selected area electron diffraction (SAED) patterns, demonstrating higher degree of crystallinity at t_{nc}=8 nm compared to 5 nm. (a-ii) and (b-ii) The high resolution TEM micrographs exhibiting lattice planes of arbitrarily selected Si-ncs. (a-iii) and (b-iii) The corresponding histograms illustrating Gaussian like size distributions of the Si-ncs.

Journal Name

ARTICLE

infer from the TEM studies that high density (~10^{10} cm^{-2}) Si-ncs of size in the order of the thickness of the nc-Si:H active layers (t_{nc}), bound by a-Si:H barrier layers, could be grown within very low thickness of a-Si:H/nc-Si:H SL thin films, while the overall crystallinity of the SL film increases rapidly and size distribution broadens with increasing t_{nc}, which grossly corroborates with the Raman results discussed earlier.

UV-VIS spectroscopy and Optical Band Gap

Based on the structural analysis by SAX, Raman and TEM, it is arguably expected that the size reduction of the Si-ncs governed by the reduced stacking thickness (t_{nc}) of the nc-Si:H active layers would pertinently control the optical properties of the superlattice thin films, e.g., absorption coefficient (α) and optical band gap (E_g). In this investigation the optical absorption coefficient spectra of the SL-films with different t_{nc} have been obtained utilizing both the reflectance and transmittance data in the UV-vis region and have been presented in Figure 5, along with the same for the bulk nc-Si:H and a-Si:H films when deposited individually. Looking at the absorption spectrum of the a-Si:H film two different energy regions are identified around 2.65 eV. The a-Si:H films do possess the highest optical absorption that increases at higher energies up to 2.65 eV beyond which a virtual saturation in optical absorption is evident. While in case of bulk nc-Si:H films similar virtual saturation seem to arise at energies above around 3.10 eV, below which the ascending absorption co-efficient values remain at magnitudes lower than those of a-Si:H network.

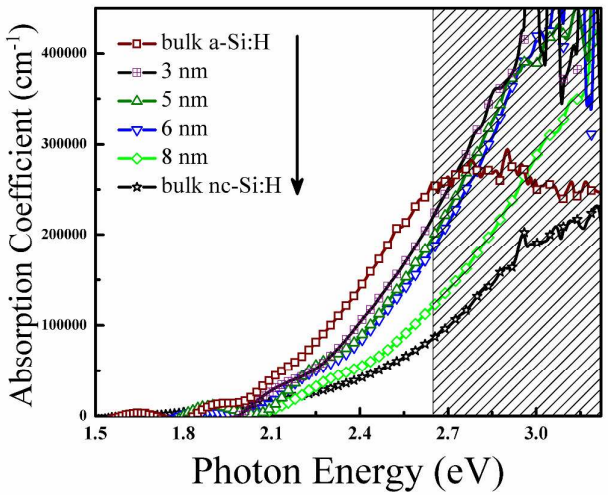

Figure 5. The optical absorption coefficient (α) spectra of the a-Si:H/nc-Si:H superlattice thin films with different thickness of nc-Si:H layer (t_{nc}).

On the formation of superlattice structure by introducing thin nc-Si:H layers of t_{nc}=3 nm, within identical a-Si:H layers of constant 4.8 nm thickness on both sides, the absorption coefficient grossly reduced for energies < 2.65 eV, beyond which, however, the absorption continues to increase monotonically on same spirit with energy. On further systematic increase in t_{nc} to 8 nm, the entire optical absorption coefficient spectra gradually reduced in intensity, showing prominent response in both below and above 2.65 eV energy regions, in a way similar to the nature of optical absorption exhibited by the single-layer nc-Si:H thin film. Accordingly, it has been identified that with the addition of even very thin nc-Si:H layers in between two a-Si:H barrier layers, the superlattice structure adopts the nc-Si characteristics in view of ascending optical absorption at higher energies beyond 2.65 eV, while maintaining the a-Si characteristics considering its magnitude higher than that of nc-Si:H layers all along. Shift in the energy ($E_{\alpha sat}$) corresponding to the saturation absorption co-efficient (α_{sat}) related to increasing t_{nc}, the thickness of the nc-Si:H active layer of the a-Si:H/nc-Si:H SL-films are shown in Table I. The results demonstrate that in case of the superlattice films of increasing t_{nc} the energy ($E_{\alpha sat}$), corresponding to the saturation absorption co-efficient (α_{sat}), gradually approaches the same for the bulk nc-Si:H film and increases even further beyond for t_{nc} > 5 nm, while the gradually increasing magnitude of α_{sat} starts reducing at t_{nc} > 5 nm. At increasing t_{nc} beyond 5 nm gradually enhanced population of the nc-Si:H component in the SL-film induces in systematic lowering of the overall absorption spectrum, thereby reducing α_{sat}, while quantum confinement effects associated to small dimensional Si-ncs in SL films of high crystallinity induces in increasing the magnitude of $E_{\alpha sat}$ beyond the same for the bulk layer nc-Si films.

Table I. Variation of the saturated absorption co-efficient (α_{sat}) and the corresponding energy ($E_{\alpha sat}$) at α_{sat}.

Bulk-layer	Superlattice t_{nc} (nm)	Saturation Absorption Coefficient (α_{sat} in cm^{-1})	Energy at α_{sat} (in eV)
a-Si:H		258793	2.65
	3	377430	2.91
	4	391247	2.93
	5	420234	2.96
	6	377430	3.00
	8	351447	3.14
nc-Si:H		193787	2.96

The optical gaps (E_g) of the SL-films were calculated using the Tauc equation $(\alpha h\nu)^{1/2} = B(h\nu - E_g)$ for allowed indirect transitions, where B is a constant known as the edge width parameter which indicates the sharpness of the band edge.[26] It is related to the width of the band tails or disorder in the film in terms of bond angle and bond length distribution.[27] The constant B, obtained from the slope of the Tauc's plot and shown in Figure 6, has been found to increase monotonically on narrowing in t_{nc}, however, a sharp increase in B has been identified at t_{nc} reducing from 8 to 6 nm which incidentally corresponds closely to the Bohr radius of Si. Usually, B is inversely proportional to the width of the tail states, which enlarges with increase in disorder. Therefore, the enhanced magnitude of B with decreasing t_{nc} implies the growth of lower defects and disorders, which might be correlated with the overall reduction of crystalline volume fraction wherein the tiny size of Si-ncs and their reduced number density altogether reduces the contribution of defects arising from related grain boundary zone. The lowering of the defects at thinner t_{nc} in SL-thin films appears advantageous in view of its potential application as absorber layer in solar cells.

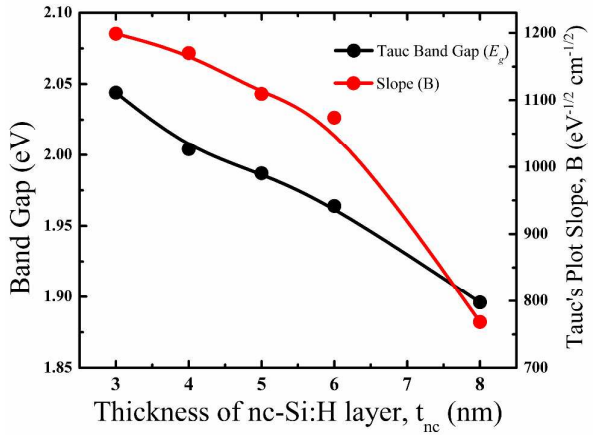

Figure 6. The gradual decaying of the optical band gap E_g and the slope B of the superlattice thin films at higher t_{nc}.

The Tauc band gap, E_g, of the SL-thin film having t_{nc}=8 nm has been estimated to be ~1.89 eV and gradual decrease in t_{nc} widens the band gap up to 2.04 eV at t_{nc}=3 nm (Figure: 6). It is remarkably noted that the optical band gaps of the superlattice thin films for 3nm $\leq t_{nc} \leq$ 8 nm are even higher than those of the bulk a-Si:H and nc-Si:H layers when deposited separately; which are ~1.85 eV for a-Si:H and ~1.64 eV for nc-Si:H thin films.

Discussions

The optical band gap of the a-Si:H/nc-Si:H SL thin films could be simply written as:

$$E_g = E_a + E_{nc},$$

where the E_a part corresponds to the band gap of the amorphous component which depends on its defect distribution and the bonded H-content, while the second term, E_{nc}, corresponds to the nano-crystalline network with varied crystalline volume fraction and changes in the average sizes of Si-ncs which are determined by the thickness (t_{nc}) of the nano-crystalline layer of individual SL-thin films in the present study.[10] It is remarkable to observe that the optical gaps of the SL-thin films are much higher than that of the a-Si:H thin films which usually possess significant amount of bonded-H that helps widening the optical gap.[28,29] For 3 nm $\leq t_{nc} \leq$ 8 nm, the SL-thin films possess reasonably high crystallinity in the range 42% $\leq F_c \leq$ 67%. The lowering in overall crystallinity of the SL-film arises due to the lower volume percentage of the nc-Si:H layer in the ensemble because of reduced t_{nc}. The a-Si:H component of the SL-film remaining unchanged in layer-thickness (t_a), changes in the nature of H-bonding and its qualitative involvement in the resultant widening of the optical gap of the SL-film is categorically excluded. Hence, predominant contribution of the nc-Si component to the optical gap, (E_{nc}), of the SL-film appears strongly evident. The E_{nc} component depends on the size of the Si-ncs due to the contribution of the quantum confinement effect.[30]

Semiconductor nanostructures exhibit increased oscillator strength due to electron hole wave function overlap. Quantum confinement (QC) is defined as the modification in the free particle dispersion relation as a function of a system's spatial dimension.[31] The confinement potential is determined by the alignment of the respective Fermi levels when a material of a band gap E_{G1} is surrounded by a material of another band gap E_{G2}, with $E_{G1}<E_{G2}$, as in the present case each nc-Si:H layer is surrounded by the a-Si:H layers on both sides.[32]

Si is an indirect gap material, meaning that, in principle, phonon scattering events are essential to maintain momentum and energy conservation during a radiative event. This situation is true in the case of a bulk material; however, as the dimension of the system is reduced, the uncertainty in the momentum k vector is increased. Therefore, it is possible to break the k selection rules making the band gap "pseudo-direct," allowing for direct e-h recombination.[33] The length scale at which this "pseudo-direct" phenomenon becomes important is typically less than a few nanometers.[34] This length scale corresponds to the systems considered here i.e., the thickness of the individual a-Si:H and nc-Si:H layers; therefore, theoretically it is valid to assume direct e-h recombination without phonon-assistance.

Considering the effective mass approximation (EMA) based on the Bloch periodic function, the exciton Bohr radius of Si is ~4.5 nm. The Bohr radius defines the spatial dimension of the particles, which determines the range of sizes for which QC can be observed. When the Si-nc size is larger than the corresponding Bohr radius, the optical gap depends only on the energy difference between the conduction and valance bands. However, when the particle size is close to the Bohr radius of the material (< 5 nm) quantum confinement and Coulomb correlation effects begin to influence the excitation energy across the band gap. As a result, the optical band gap is no longer independent of particle size rather it is inversely proportional to the square of the radius of Si-ncs. This confinement effect leads to the sharp widening of the E_{nc} component for tiny size of Si-ncs which is a consequence of the decreasing t_{nc}.[35, 36] Similar changes in the optical absorption and the corresponding widening in the optical gap due to the quantum size effects were identified in

Si-ncs obtained from stacked layer Si:H films deposited by interrupted growth and H-plasma treatment.[37, 38]

Considering the experimentally obtained constants e.g., saturation absorption co-efficient (α_{sat}), the corresponding energy ($E_{\alpha sat}$), the edge width parameter (B) and the estimated optical gap (E_g), and in view of the quantum confinement effects controlling the optical phenomena, the effective density of states distributions and their relative nature of variations on the periodic stacking thickness (t_{nc}) of the nc-Si:H active layers in the a-Si:H/nc-Si:H superlattice thin films can be empirically presented as in Figure 7. In a quantum mechanical pseudo-potential calculation, Wang *et. al.* have shown that the magnitude of the local density of states increases beyond the band edges with simultaneous increase in the energy corresponding to its virtual saturation when the silicon quantum dots becomes larger in size.[39] In reliance with that report elevated magnitude of the saturation optical absorption co-efficient, α_{sat}, with increasing t_{nc} in our superlattice films demonstrates enhanced effective density of states along with the increase in the corresponding $E_{\alpha sat}$. However, for $t_{nc} \geq 8$ nm, the magnitude of the saturation

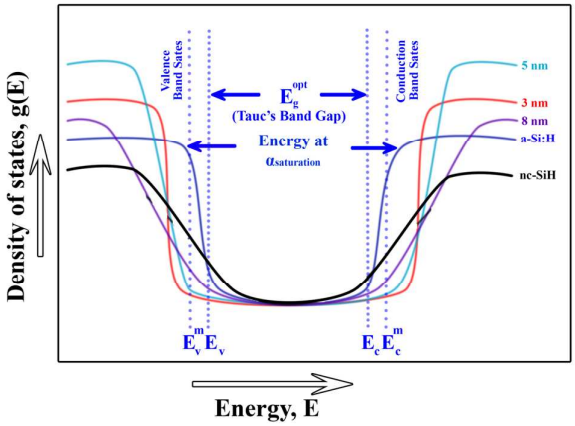

Figure 7. Empirical density of states distribution and their nature of variations on the stacking thickness (t_{nc}) of the nc-Si:H active layers in the a-Si:H/nc-Si:H superlattice thin films.

density of states have reduced with simultaneous lowering in $E_{\alpha sat}$, because of the effectively feeble confinement effects with size of the Si-ncs ~ 7.5 nm.

Optimization on the optical properties of a-Si:H/nc-Si:H superlattice structures, discarding the conventional post-deposition high-temperature annealing steps, will be of immense importance in further developments in all-silicon solar cells. In this regard, there are only very few reports available in the literature.[40,41] In such a work by *Liu et. al.*, the alternate layers of μc-Si:H and a-Si:H were deposited within capacitively and inductively coupled electrodes, respectively which certainly made the deposition steps further complicated.

In the present investigation, a single-step low temperature yet simple and most popular capacitively coupled PECVD technique have been utilized to fabricate a-Si:H/nc-Si:H in super-lattice structures. While, preparing silicon nano-crystals embedded within amorphous silicon matrix at low temperature, the re-etching of the growing film surface by the atomic hydrogen present in the plasma is the predominant factor. The growth of silicon thin-films, from SiH_n radicals in the plasma, begins with an incubation layer on the substrate surface and that happens to be mostly defective and amorphous in nature, because of the inherent lattice mismatch between the substrate material and the interacting Si precursors.[42] The typical thickness for such incubation layer on glass substrate, at the most crystalline-prone deposition conditions, varies between several tens of nano-meters beyond which nano-crystallization starts occurring. This incubation layer usually becomes the perpetual hindrance for the formation of nc-Si:H network within layers of thickness ~3-8 nm. In the present set of samples, this obstacle has been surpassed by the initial deposition of an amorphous silicon sub-layer on the substrate, followed by the deposition of nc-Si:H layer. This initial a-Si:H sub-layer acts as the virtual incubation layer to the growth of Si-ncs and that effectively eliminates the real incubation layer for the growth of Si-ncs within the nc-Si:H sub-layer, in the present parametric deposition conditions. As a result, a significantly high crystallinity was attained even within its very low thickness as low as 3 nm. The size of the Si-ncs has been controlled by the interruption of growth of the nc-Si:H sub-layer, by allowing the next cycle of a-Si:H sub-layer to grow. This process of crystallization by providing virtual incubation layer from the a-Si:H barrier layer and interruption of growth of nc-Si:H layer was repeated to fabricate the superlattice structure. While, the diffraction peaks of SAX validates the formation of superlattice structure consisting of alternative layers of a-Si:H and nc-Si:H, the Raman studies have shown a consistent reduction of the Si-nc size from 7.5 nm to 3.9 nm, as t_{nc} is reduced from 8 nm to 3 nm. Thus, in layer-by-layer deposition the a-Si:H layers of identical thickness provide the amorphous virtual incubation layer and the growth interruption of the nc-Si:H layers of limiting layer-thickness controls the size of Si-ncs and the overall crystallinity of the superlattice structure.

The miniaturization of the size of Si-ncs have been found to be very effective in tuning the optical properties (absorption coefficient and optical band gap) of the SL-thin films without any inclusion of foreign elements (O/C/N) in the pristine crystalline silicon network. For thin films with $3 \leq t_{nc}$ (nm) ≤ 6, the optical absorption coefficients have very high magnitude at higher photon energy which ensures better light absorption compared to its amorphous part. Moreover, the existence of nano-crystallites can diminish the light induced degradation and enhance quantum efficiency at the infra-red range. Although, the band gap is widened with reduction of the size of Si-ncs, the presence of nano-crystallites can enable the conduction charge carriers through the tunnelling between the Si-ncs. In addition, the a-S:H/nc-Si:H SL-thin films do possess a low concentration of defects which altogether facilitates its potential applications in solar cells.

Conclusions

Superlattice films consisting of repeated cycles of alternate a-Si:H barrier-layer and nc-Si:H active-layer of stacking thickness t_a and t_{nc}, respectively have been prepared from the (SiH_4 + H_2)-plasma in a capacitively coupled PE-CVD system at a moderately low

temperature of 180 ^{o}C. Formation of the superlattice structure has been confirmed by the small angle XRD data, while the average size of the Si-ncs along with the gross crystalline volume fraction of the films have been estimated from the Raman spectroscopy data. The crystallographic orientations of the Si-ncs have been identified from the X-ray diffraction results and the electron diffraction pattern, while the size of the Si nanocrystallites are further confirmed from the histogram plot in TEM data. It has been demonstrated how the variation in the stacking thickness (t_{nc}) of the nc-Si:H layer can grossly modify the overall structural and optical properties of the superlattice thin films. The average size (d in nm) of Si-ncs closely resembles with the nc-S:H active layer thickness (t_{nc} in nm) whereas, the width of the size distribution of the Si-ncs and their crystalline volume fraction change proportionally with t_{nc}. With the thinning of the nc-Si:H layer from 8 nm to 3 nm the crystalline volume fraction reduces from 67.4% to 42%, while the optical absorption has grossly increased at photon energies above 2.65 eV along with simultaneous widening in the optical band gap from 1.89 eV to 2.04 eV as contributed by the quantum size effect on Si nanocrystallites. Changing slope of the optical absorption edge identifies the lowering of defects in the superlattice thin films at lower thickness of the nc-Si:H sub-layer which also have been corroborated from the Raman studies. High optical absorption in the towards-UV part of the solar spectrum with simultaneous widening in the optical gap and lowering in the defect states identifies the nc-Si:H/a-Si:H superlattice thin films as a superior material for using in different *i*-layers in the triple junction all silicon solar cells. The successful formation of Si-ncs even within very thin nc-Si:H layers has been instrumental by the initial deposition of a-Si:H layer which acts as a virtual incubation layer to the growth of nano-crystalline sub-layer under chosen parametric condition. Ensuing plasma deposition technique for the fabrication of Si-ncs within superlattice thin films by plasma enhance CVD system at low temperature is significantly effective in tuning of its structural and optical characteristics as an advanced material for prospective applications in numerous photonic and opto-electronic devices.

Acknowledgements

The work has been done under nano-silicon projects funded by the Department of Science and Technology (Nano-Mission Program) and the Council of Scientific and Industrial Research, Government of India. The HR-TEM studies have been performed using facilities of the Unit on Nano-Science at IACS.

References

[1] M. Cazzanelli, D. Navarro-Urriós, F. Riboli, N. Daldosso, L. Pavesi, J. Heitmann, L. X. Yi, R. Scholz, M. Zacharias and U. Gösele, *J. Appl. Phys.* 2004, **96**, 3164-3171.

[2] B. Dridi Rezgui, F. Gourbilleau, D. Maestre, O. Palais, A. Sibai, M. Lemiti and G. Brémond, *J. Appl. Phys.* 2012, **112**, 024324.

[3] L. Pavesi, L. Dal Negro, C. Mazzoleni, G. Franzo and F. Priolo, *Nature* 2000, **408**, 440-444.

[4] D. Das and A. Samanta, *Nanotechnology* 2011, **22**, 055601.

[5] D. Di, I. Perez-Wurfl, L. Wu, Y. Huang, A. Marconi, A. Tengattini, A. Anopchenko, L. Pavesi and G. Conibeer, *Appl. Phys. Lett.* 2011, **99**, 251113.

[6] J. M. Shieh, W. C. Yu, J. Y. Huang, C. K. Wang, B. T. Dai, H. Y. Jhan, C. W. Hsu, H. C. Kuo, F. L. Yang and C. L. Pan, *Appl. Phys. Lett.* 2009, **94**, 241108.

[7] X. J. Hao, A. P. Podhorodecki, Y. S. Shen, G. Zatryb, J. Misiewicz and M. A. Green, *Nanotechnology*, 2009, **20**, 485703.

[8] I. A. Yunaz, K. Hashizume, S. Miyajima, A. Yamada and M. Konagai, *Sol. Energ. Mat. Sol. Cells*, 2009, **93**, 1056-1061.

[9] A. Samanta and D. Das, *J. Mat. Chem.* 2011, **21**, 7452-7458.

[10] D. Kar and D. Das, *J. Mat. Chem. A.* 2013, **1**, 14744-14753.

[11] B. Sain and D. Das, *Phys. Chem. Chem. Phys.* 2013, **15**, 3881-3888.

[12] Q. Cheng, S. Xu, S. Huang and K. Ostrikov, *Crys. Growth Design.* 2009, **9**, 2863-2867.

[13] S. Park, E. Cho, D. Song, G. Conibeer, M. A. Green, *Sol. Energ. Mat. Sol. Cells,* 2009, **93**, 684-690.

[14] G. Scardera, T. Puzzer, I. Perez-Wurfl and G. Conibeer, *J. Cryst. Growth.* 2008, **310**, 3680-3684.

[15] D. Song, E. C. Cho, G. Conibeer, Y. Huang, C. Flynn and M. A. Green, *J. Appl. Phys.* 2008, **103**, 083544.

[16] B. G. Lee, D. Hiller, J. W. Luo, O. E. Semonin, M. C. Beard, M. Zacharias and P. Stradins, *Adv. Funct. Mater.* 2012, **22**, 3223-3232.

[17] Y. Rosenwaks, M. C. Hanna, D. H. Levi, D. M. Szmyd, R. K. Ahrenkiel and A. J. Nozik, *Phys. Rev. B.* 1993, **48**, 14675-14678.

[18] Z. Li, W. Li, Y. Jiang, H. Cai, Y. Gong and J. He, *J. Raman Spectrosc.* 2011, **42**, 415-421.

[19] D. Raha and D. Das, *Sol. Energ. Mat. Sol. Cells,* 2011, **95**, 3181-3188.

[20] M. Jana, D. Das and A. K. Barua, *Sol. Energ. Mat. Sol. Cells,* 2002, **74**, 407-413.

[21] S. Guha, G. Hendershot, D. Peebles, P. Steiner, F. Kozlowski and W. Lang, *Appl. Phys. Lett.* 1994, **64**, 613-615.

[22] D. Das, *Thin Solid Films*. 2005, **476**, 237-245.

[23] B. Sain and D. Das, *Sci. Adv. Mat.* 2013, **5**, 188.

[24] D. Das and D. Kar, *Phys. Chem. Chem. Phys.* 2014, **16**, 25421-25431.

[25] W. Ke, X. Feng and Y. Huang, *J. Appl. Phys.* 2011, **109**, 083526.

[26] A. R. Kadir,R. A. Rani, M. Alsaif, J. Z. Ou, W. Wlodarski, A. P. O'Mullane and K. Kalantar-zadeh, *Appl. Mater. Inter.* 2015, **7**, 4751–4758.

[27] K. Bhattacharya and D. Das, *J. Phys. D: Appl. Phys*. 2008, **41**, 155420.

[28] H. Águas, V. Silva, E. Fortunato, S. Lebib, P. Roca i Cabarrocas, I. Ferreira, L. Guimarães and R. Martins, *Jpn. J. Appl. Phys*. 2003, **42**, 4935–4942.

[29] D. Das, *Bull. Mater. Sci.* 1997, **20**, 9–22.

[30] D. Das, *Jpn. J. Appl. Phys*. 1994, **33**, L571–L574.

[31] A. D. Yoffe, *Adv. Phys*. 2002, **51**, 799.

[32] W. R. Frensley and H. Kroemer, *Phys. Rev. B*. 1977, **16**, 2642.

[33] D. Kovalev, H. Heckler, M. Ben-Chorin, G. Polisski, M. Schwartzkopff and F. Koch, *Phys. Rev. Lett.* 1998, **81**, 2803.

[34] M. S. Hybertsen, *Phys. Rev. Lett.* 1994, **72**, 1514.

[35] M. B. Sahana, C. Sudakar, A. Dixit, J. S. Thakur, R. Naik and V. M. Naik, *Acta Mater.* 2012, **60**, 1072-1078.

[36] T. Rajagopalan, X. Wang, B. Lahlouh, C. Ramkumar, P. Dutta and S. Gangopadhyay, *J. Appl. Phys.* 2003, **94**, 5252-5260.

[37] D. Das, *Solid State Commun.* 1998, **108**, 983-987.

[38] D. Das and M. Jana, *Sol. Energ. Mat. Sol. Cells,* 2004, **81**, 169-181.

[39] L. W. Wang and A. Zunger, *Phys. Rev. Lett.* 1994, **73**, 1039.

[40] J. Ma, J. Ni, J. Zhang, Q. Liu, G. Hou, X. Chen, X. Zhang and Y. Zhao, *Sol. Energ. Mat. Sol. Cells,* 2014, **123**, 228-232.

[41] J. Liu and L. Feng, *Appl. Phys. Lett.* 1993, **63**, 2783-2785.

[42] D. Das, *Solid State Phen.* 1995, **44**, 227-258.